Bioorganic Chemistry 113 (2021) 105022

Contents lists available at ScienceDirect

Bioorganic Chemistry

journal homepage: www.elsevier.com/locate/bioorg

Identification of *ortho* catechol-containing isoflavone as a privileged scaffold that directly prevents the aggregation of both amyloid β plaques and tau-mediated neurofibrillary tangles and its in vivo evaluation

Seung Hwan Son [a,1], Ji Min Do [b,1], Ji-Na Yoo [c,d,1], Hyun Woo Lee [a], Nam Kwon Kim [e], Hyung-Seok Yoo [a], Min Sung Gee [a], Jong-Ho Kim [a], Ji Hye Seong [f], Kyung-Soo Inn [a,e], Min-Duk Seo [c,d,*], Jong Kil Lee [a,*], Nam-Jung Kim [a,e,*]

[a] College of Pharmacy, Kyung Hee University, Seoul 02447, Republic of Korea
[b] Department of Biomedical Science and Technology, Graduate School, Kyung Hee University, Seoul 02447, Republic of Korea
[c] College of Pharmacy and Research Institute of Pharmaceutical Science and Technology (RIPST), Ajou University, Suwon 16499, Republic of Korea
[d] Department of Molecular Science and Technology, Ajou University, Suwon 16499, Republic of Korea
[e] Department of Life and Nanopharmaceutical Sciences, Graduate School, Kyung Hee University, Seoul 02447, Republic of Korea
[f] Brain Science Institute, Korea Institute of Science and Technology (KIST), Seoul 02792, Republic of Korea

ARTICLE INFO

Keywords:
Polyhydroxyisoflavone
Amyloid β
Tau
Alzheimer's disease
Catechol

ABSTRACT

In this study, polyhydroxyisoflavones that directly prevent the aggregation of both amyloid β (Aβ) and tau were expediently synthesized via divergent Pd(0)-catalyzed Suzuki-Miyaura coupling and then biologically evaluated. By preliminary structure–activity relationship studies using thioflavin T (ThT) assays, an *ortho*-catechol containing isoflavone scaffold was proven to be crucial for preventing both Aβ aggregation and tau-mediated neurofibrillary tangle formation. Additional TEM experiment confirmed that *ortho*-catechol containing isoflavone **4d** significantly prevented the aggregation of both Aβ and tau. To investigate the mode of action (MOA) of **4d**, which possesses an *ortho*-catechol moiety, ^{1}H-^{15}N HSQC NMR analysis was thoroughly performed and the result indicated that **4d** could directly inhibit both the formation of $A\beta_{42}$ fibrils and the formation of tau-derived neurofibrils, probably through the catechol-mediated nucleation of tau. Finally, **4d** was demonstrated to alleviate cognitive impairment and pathologies related to Alzheimer's disease in a 5XFAD transgenic mouse model.

1. Introduction

Alzheimer's disease (AD) is a progressive and irreversible neurodegenerative disorder characterized by cognitive impairment, memory loss, and continuous decline in behavioral and social skills [1,2]. In 2018, prevalence of the disease was reached to about 50 million patients worldwide, and it is expected that this number will more than triple to 152 million by 2050 [3]. A few drugs are currently approved and are used clinically to alleviate the symptoms of AD [4,5]. These medications are generally classified into 2 groups that attenuate symptoms in different ways: acetylcholinesterase (AchE) inhibitors and *N*-methyl-D-aspartic acid receptor (NMDAR) antagonists. Unfortunately, while both types of drugs help reduce the symptoms of AD, neither drugs cure the disease nor effectively delay its progression [1]. Therefore, a breakthrough is urgently needed for the treatment of this disease. The cause of AD is largely unknown, but it is worsened by abnormal accumulation of pathological proteins such as amyloid β (Aβ) and tau-mediated neurofibrillary tangles (NFT) [6–11]. However, various targeting strategies for pathological proteins, especially Aβ, using monoclonal antibodies (mAbs) have not been successful [12,13]. Recently, oligomeric Aβ and its plaques have been considered to play crucial roles in AD-associated pathological toxicity [14–19]. The tau monomer is also known to be nontoxic, but its aggregated insoluble form, NFT, has been found to be neurotoxic [20–22].

Therefore, chemical prevention of the transformation of Aβ and tau monomers into toxic polymers would be valuable as a novel therapeutic strategy as well as a research tool for AD [23,24]. Isoflavones, which possess 3-phenyl-4*H*-chromen-4-one as their main skeleton, are widely

* Corresponding authors.
E-mail addresses: mdseo@ajou.ac.kr (M.-D. Seo), jklee3984@khu.ac.kr (J.K. Lee), kimnj@khu.ac.kr (N.-J. Kim).
[1] These authors contributed equally.

https://doi.org/10.1016/j.bioorg.2021.105022
Received 5 November 2020; Received in revised form 3 April 2021; Accepted 23 May 2021
Available online 26 May 2021

occurring natural flavonoids and synthetic derivatives [25–29]. Interestingly, a series of polyhydroxyisoflavones such as daidzein **4a** were recently identified as novel therapeutic scaffolds for AD [30–39]. Especially, they exhibited to reduce the amount of Aβ and tau that are sometimes pathologically aggregated in AD model. However, a detailed study on polyhydroxyisoflavones has not yet been performed to investigate their biological ability to directly prevent pathologically aggregated forms of both Aβ and tau in vitro or alleviate AD in vivo.

2. Results and discussion

The structurally rigid features of polyhydroxyflavonoids and their H-bonding formation abilities make the privileged structures prevent Aβ aggregation through their direct binding and destabilizing aggregating conformation. Recently, a series of pioneering works that metal-associated Aβ aggregation could be inhibited by isoflavone with *ortho*-catechol supported the significance of the skeleton as a template for the novel inhibitor preventing the aggregation of pathological proteins such as Aβ [40–48]. In addition, *ortho*-catechol moiety can directly bind tau proteins and prevent their aggregation in AD [49]. Inspired by the previous reports, we rationally designed and synthesized a series of isoflavones, focusing on the incorporation of an *ortho*-catechol moiety that make H-bonding or coordinate binding with metal such as Cu^{2+}. And we evaluated their ability to prevent the aggregation of Aβ and tau using in vitro biochemical assay, and elucidated that the *ortho*-catechol containing polyhydroxyisoflavones could inhibit the aggregation of both pathological proteins. Finally, we showed that isoflavone **4d**, which possesses the pharmacophore, alleviates both cognitive impairment and the pathologies related to AD in an in vivo 5XFAD transgenic mouse model. Thus, this small molecule compound that directly prevents aggregation of both pathological proteins was identified in vitro and shown to alleviate pathology in vivo [50,51].

Polyhydroxyisoflavones **3f-g** and **4a-e** were expediently synthesized via 2-step reactions from 3-bromo-4*H*-chromen-4-one **1**, involving Suzuki-Miyaura coupling [52] and sequential demethylation (Scheme 1). 3-bromo-4*H*-chromen-4-one **1a** and **1b** was prepared from commercially available compound **5a** and **5b** via sequential acetylation and bromination (Scheme 2).

With polyhydroxyisoflavones in hand, we investigated whether the compounds could prevent $Aβ_{42}$ aggregation using the biochemical ThT assay (Fig. 1A). A solution of monomeric $Aβ_{42}$ (10 μM) in HEPES buffer was incubated in the absence or presence of polyhydroxyisoflavones (30 μM), and the extent of aggregation was monitored by ThT fluorescence. In the experiment, we found that **4c**, **4d** and **4e**, 3′,4′-dihydroxyisoflavones possessing *ortho*-catechol moiety, could prevent $Aβ_{42}$ aggregation in both of the metal-free condition and metal (Cu^{2+} or Zn^{2+})-treated conditions (Fig. 1 and S1). In addition, Cu^{2+}-mediated Aβ aggregation (Fig. 1A. Right Panel) was more likely to be prevented, compared with metal-free Aβ aggregation (Fig. 1B. Right Panel) in the normalized fluorescence intensity of Aβ ThT assay (Fig. S2) at 24 h after the treatment of 3′,4′-dihydroxyisoflavones such as **4d**. It seems that the compounds can prevent metal free Aβ aggregation and more significantly prevent Cu^{2+}-mediated Aβ aggregation by the additional enforcement. To confirm whether the additional interacting activity of 3′,4′-dihydroxyisoflavones would be involved with its metal binding potential, we performed the additional experiment using UV/Vis spectrophotometry. In the result, we observed that **4d**, one of 3′,4′-dihydroxyisoflavones could have potential interacting with Cu^{2+}. When Cu^{2+} was added to the aqueous solution of **4d**, spectral change was detected (Fig. S3) and this result was in coincidence with the previous reports on the interaction between metal and its potential binders [41]. Therefore, it is plausible that 3′,4′-dihydroxyisoflavones might bind Cu^{2+} and consequently interfere with the interaction between $Aβ_{42}$ and Cu^{2+}, leading to the prevention of Aβ aggregation. In addition, 3′,4′-dihydroxyisoflavone **4d** showed the Aβ aggregation preventive activity more or equipotent to epigallocatechin gallate (EGCG), a known compound having anti-Aβ aggregation effect (Fig. S4) [53–56].

Next, we investigated the preventive effect of polyhydroxyisoflavones on tau aggregation. Similar to the $Aβ_{42}$ aggregation assay, recombinant tau (2N4R, 10 μM) was treated with polyhydroxyisoflavones (30 μM) (Fig. 2). We confirmed that catechol containing isoflavones (**4c**, **4d** and **4e**) also caused significant reductions in heparin-induced ThT fluorescence. Among the 3′,4′-dihydroxyisoflavones, **4d** showed the best inhibitory activity for tau aggregation in the biochemical assay. Based on the inhibitory effect on both $Aβ_{42}$ and tau aggregation, we chose **4d** as a chemical probe for further study. In addition, the anti-aggregation

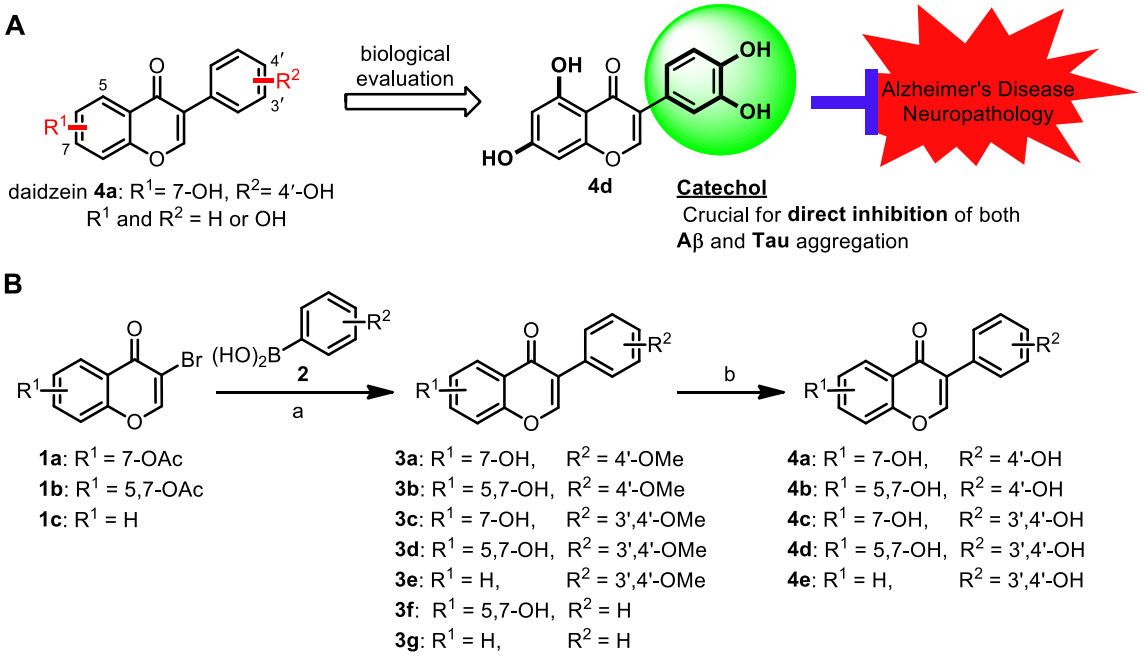

Scheme 1. Design and synthesis of polyhydroxyisoflavones **3f-g** and **4a-e**. Reagents and reaction conditions: a) **2**, $Pd(OAc)_2$, SPhos, K_2CO_3, DMF/H_2O (3:1), 90 °C; b) Pyr·HCl, reflux.

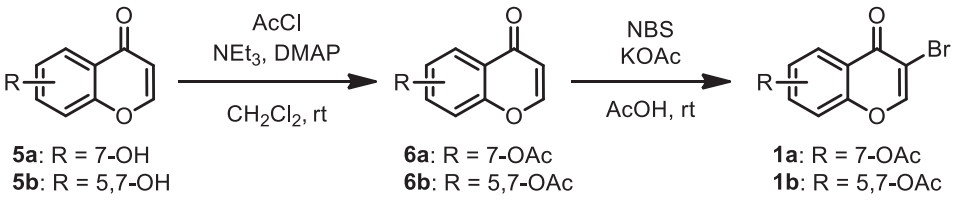

Scheme 2. Synthetic scheme of 3-bromochromone **1a** and **1b**.

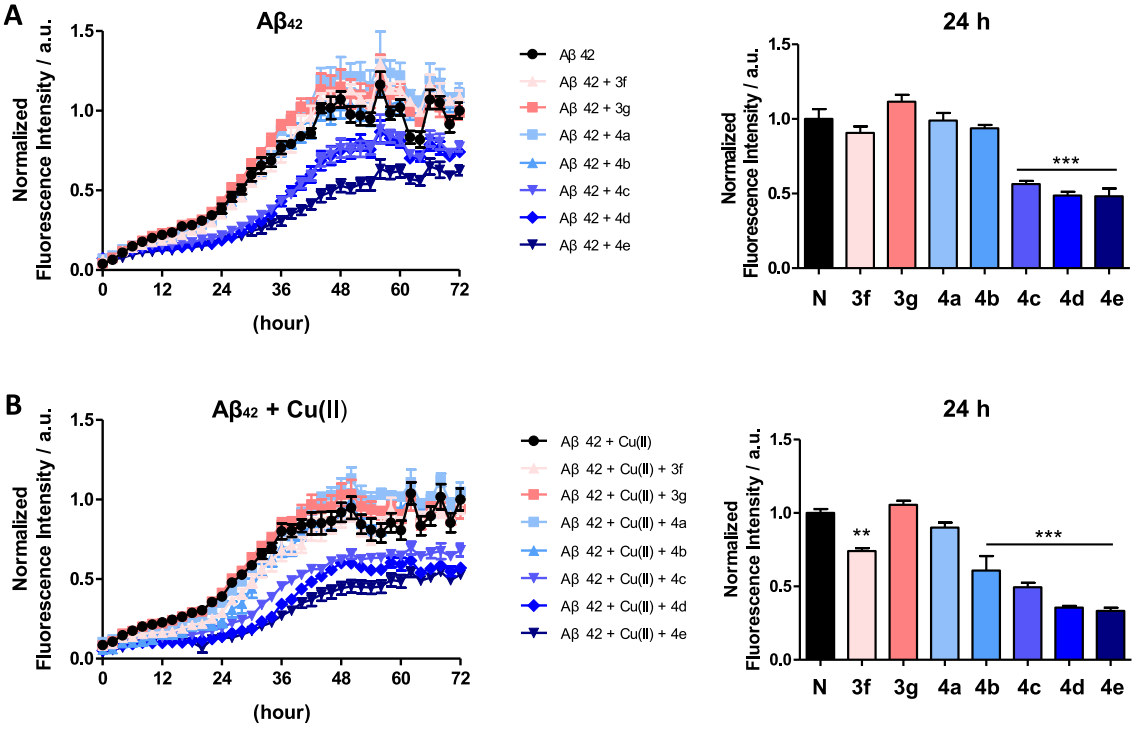

Fig. 1. Effects of polyhydroxyisoflavones on the formation of Aβ aggregates. (A and B) For Aβ ThT assays examining the effect of compounds on aggregation, Aβ (10 μM) was incubated in the absence or presence of $CuCl_2$ or $ZnCl_2$ (10 μM) and compounds (30 μM) in a HEPES solution containing ThT (20 μM). The time course of aggregation (left) and simplified bar plot representation of ThT data (right) for $A\beta_{42}$ in the metal-free condition (A) and the presence of Cu^{2+} (B) (n = 6 per group). Data are shown as the mean ± SEM. One-way ANOVA. $^{**}P < 0.01$ and $^{***}P < 0.001$ vs. the nontreated group (N).

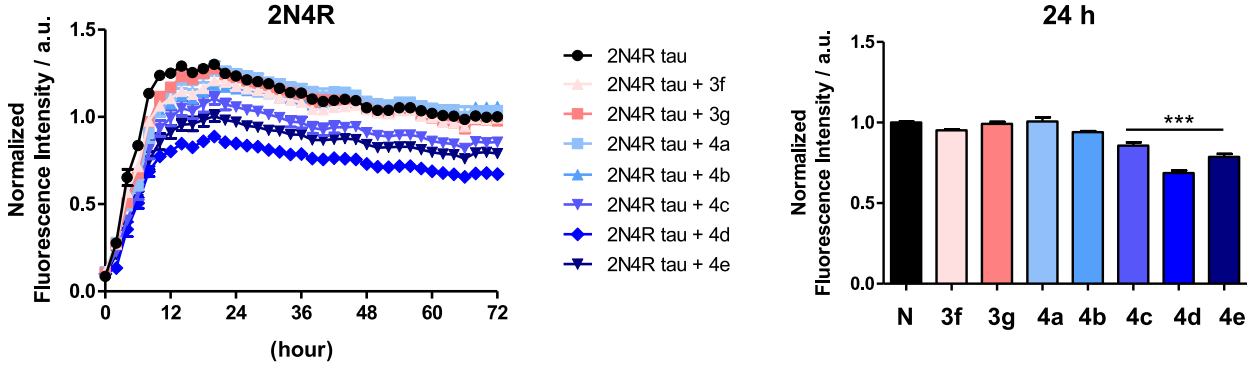

Fig. 2. Effects of polyhydroxyisoflavones on the formation of tau aggregates. For tau ThT assays examining the effect of compounds on aggregation, recombinant wild-type 2N4R tau (10 μM), compounds (30 μM) and ThT (20 μM) were mixed in the a HEPES solution. Time-dependent ThT fluorescence of heparin-induced tau aggregation (left) and simplified bar plot representation of ThT data (right) for 2N4R tau (n = 6 per group). Data are shown as the mean ± SEM. One-way ANOVA. $^{***}P < 0.001$ vs. the nontreated group (N).

effect of **4d** on Aβ and tau was shown in a concentration-dependent manner (Fig. S5).

Next, we investigated whether **4d** could prevent pathological aggregation of both $A\beta_{42}$ and tau using TEM analysis (Figs. 3 and 4). In the analysis, the images of metal-free $A\beta_{42}$ and Cu^{2+}-added $A\beta_{42}$ samples treated with **4d** revealed that pathology-related $A\beta_{42}$ aggregates, including fibrils, formed rarely (Fig. 3). In addition, tau fibril aggregates were barely observed in the sample incubating with **4d** in the

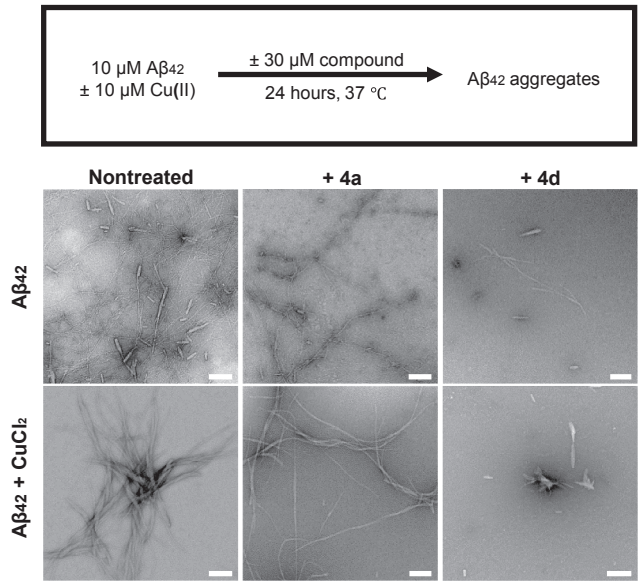

Fig. 3. Representative TEM images of Aβ. Images of the aggregated $A\beta_{42}$ in samples incubated for 24 h with **4a** and **4d** in the presence or absence of Cu^{2+} (scale bar, 500 nm).

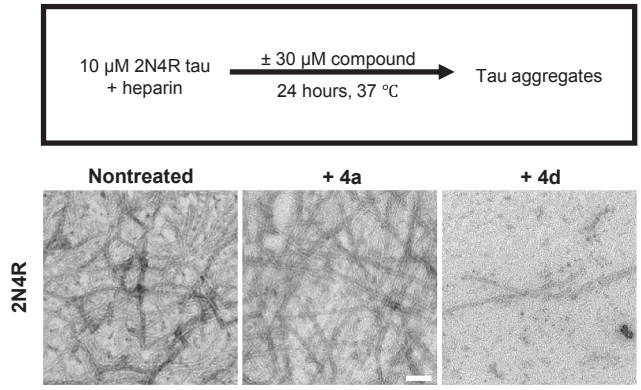

Fig. 4. Representative TEM images of tau. Images of heparin-induced 2N4R tau after a 24 h incubation with **4a** and **4d** (scale bar, 500 nm).

transmission electron microscopy (TEM) experiment (Fig. 4). However, **4a**-treated $A\beta_{42}$ samples showed a morphology similar to that of non-treated $A\beta_{42}$ samples in the presence or absence of Cu^{2+}. Tau with vehicle or **4a** also formed fibrous aggregates after 24 h of incubation. Taken together, these data indicated that **4d** could inhibit both $A\beta_{42}$ and tau aggregation.

To understand the mechanism of action of **4d** at the molecular level, we employed nuclear magnetic resonance (NMR) spectroscopy. First, **4d** was titrated to the metal-free $A\beta_{42}$ monomer or monomeric tau at various molar ratios. In the ^{1}H-^{15}N heteronuclear single quantum correlation (HSQC) spectra of $A\beta_{42}$ and tau, no significant spectral changes were detected when **4d** was added (Fig. S6). This means that **4d** might not bind directly to monomeric $A\beta_{42}$ or monomeric tau or might bind very weakly. Then, we investigated the inhibitory effects of **4d** on the aggregation of $A\beta_{42}$. After incubation at 25 °C with shaking for 4 h, a reaction condition known to induce rapid protein aggregation, most of the cross peaks disappeared, indicating the formation of $A\beta_{42}$ aggregates (Fig. 5A-C). Although several peaks of amino acid residues such as F4, R5, V36, and I41 were still alive after 4 h incubation, the intensities of those peaks were very low. However, coincubation of $A\beta_{42}$ with **4d** resulted in the NMR signal different from that observed in the absence of **4d**. The intensities of all cross peaks of $A\beta_{42}$ after 4 h of coincubation were slightly reduced but there were no disappearing peaks (Fig. 5D-F), indicating that the formation of $A\beta_{42}$ fibrils was inhibited [59]. Given that all cross peaks of $A\beta_{42}$ completely disappeared after 12 h of incubation with shaking (data not shown), the NMR results suggest that **4d** can inhibit or slow down the aggregation of $A\beta_{42}$.

Next, we employed NMR to elucidate the role of **4d** in the aggregation of tau. The effect of **4d** on tau aggregation was more complicated and ambiguous than that on $A\beta_{42}$ aggregation. It is known that heparin-induced tau aggregation results in decreased signal intensities for tau, similar to the shaking experiment with $A\beta_{42}$ [60]. The time course NMR spectra of heparin-induced tau were obtained in the presence or absence of **4d** (Fig. 6). The NMR signal intensities for many peaks of tau without **4d** gradually decreased, and those peaks completely disappeared. Surprisingly, the aggregation kinetics of tau in the presence of **4d** showed significantly different patterns. Most of the perturbed peaks in the presence of **4d** showed more rapidly decreasing intensities than those in the absence of **4d** (Fig. 6A and 6B). As a result, the peaks of tau in the presence of **4d** disappeared much more quickly than those of tau without **4d** (Fig. 6C and 6D). However, a few cross-peaks of tau shown in Fig. 6E showed reverse patterns, that is, more slowly decreasing intensities and longer survival of resonances during incubation in the presence of **4d**. It was assumed that there are regional differences between the sequences that easily aggregated or were involved in the aggregation process and the other sequences, probably due to the relatively large size and random coil structure of monomeric tau. As the intensities of HSQC spectra are proportional to the tau monomer concentration, the different decreasing patterns of cross peaks of tau strongly implied that aggregation or fibrillation of tau was affected by **4d**. Tau is aggregated through either cysteine-dependent polymerization or cysteine-independent polymerization. These two types of polymerization occur and sometimes have synergistic effects on the aggregation process [61].

Recently, it was reported that blocking cysteine covalently on tau makes the protein a stable nucleated oligomer and does not lead to the formation of tau-derived neurofibrillary tangles. In TEM analysis, this nucleated form is generally observed as a globular form [62]. In particular, our TEM results clearly showed the formation of nucleated tau after treatment with compound **4d** (Fig. 4 and S7). It was reported that the *ortho*-catechol (1,2-dihydroxybenzene) moiety, a crucial pharmacophore of **4d**, can covalently bind cysteine residues on tau, preventing the aggregation process [51]. It is thought that **4d** might play a role in the aggregation process of tau, such as nucleation and oligomerization, which results in inhibition of the formation of tau-derived neurofibrils, probably through the catechol-mediated nucleation of tau. To investigate whether compound **4d** can bind a cysteine residue in a covalent manner, simple experiments in which **4d** was incubated with cycteine or *N*-acetyl cysteine were also performed. As anticipated, covalent adducts of **4d** with corresonding cysteine residues were detected by LC-MS analysis, indicating that compound **4d** might bind a cysteine residue in tau through covalent bonding (data in SI).

To examine the in vivo effects of **4d** on AD pathology, 5XFAD mice were treated with compound **4d** daily for 2 months starting at the age of 5 months (Fig. 7A) [63,64]. Compound **4a**-treated mice were used as a control group. During the treatment period, the body weights of the mice were not significantly changed, and no significant side effects were observed (data not shown). The Morris water maze (MWM) test was performed to identify defects in spatial learning and memory. The vehicle-treated 5XFAD mice consistently reached the platform later than the vehicle-treated wild-type (WT) mice, indicating that they had difficulties with learning and memory.

Remarkably, administration of **4d** to 5XFAD mice led to a significant improvement in performance in the task at days 5, 6 and 7 (Fig. 7B). At day 8, the hidden platform was removed, and a probe task was performed. The number of platform crosses increased significantly in **4d**-treated 5XFAD mice compared with vehicle-treated 5XFAD mice (Fig. 7C). The swim speed and total track length did not differ between

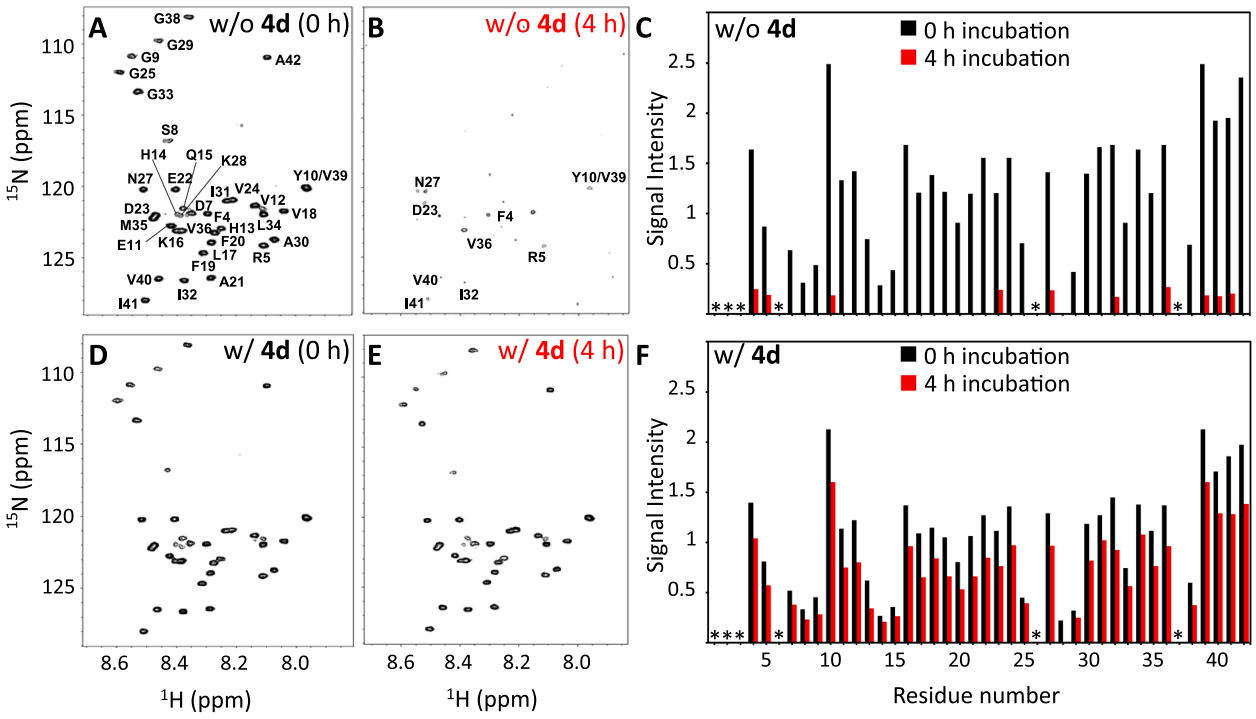

Fig. 5. Effects of **4d** on the fibrillation of $A\beta_{42}$. (A-C) The ^{1}H-^{15}N HSQC spectra of $A\beta_{42}$ in its apo-states before incubation (A) and after incubation for 4 h at 25 °C with shaking at 200 rpm (B). The intensities of the corresponding cross peaks before and after incubation are plotted in (C). (D-F) The spectra of $A\beta_{42}$ in the presence of **4d** before (D) and after incubation (E). The peak intensities of each condition are plotted in (F). The chemical shifts of $A\beta_{42}$ residues are referred from the reported backbone assignment data of $A\beta_{42}$ [57,58]. The residues that were not observed in the HSQC spectra are marked with black asterisks in (C) and (F).

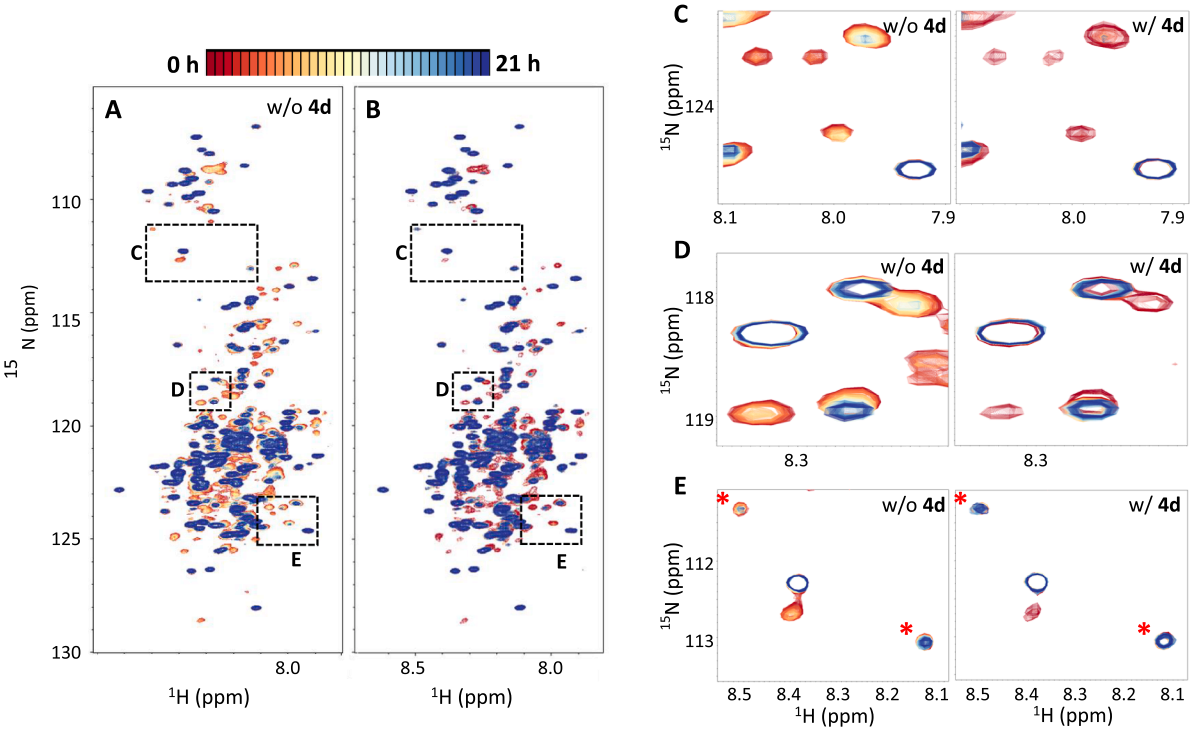

Fig. 6. Effects of **4d** on the fibrillation of tau. The time course ^{1}H-^{15}N HSQC spectra of tau in the absence (A) and presence (B) of **4d** for 21 h. Spectral measurements were started immediately after the addition of heparin. Selected regions shown in (C-E) are represented by dotted rectangles. The selected residues shoiwng rapidly decreasing intensities in the presence of **4d** are enlarged in (C) and (D). (E) The residues showing the longer survivals of resonances in the presence of **4d** are highlighted by red asterisks. (For interpretation of the references to colour in this figure legend, the reader is referred to the web version of this article.)

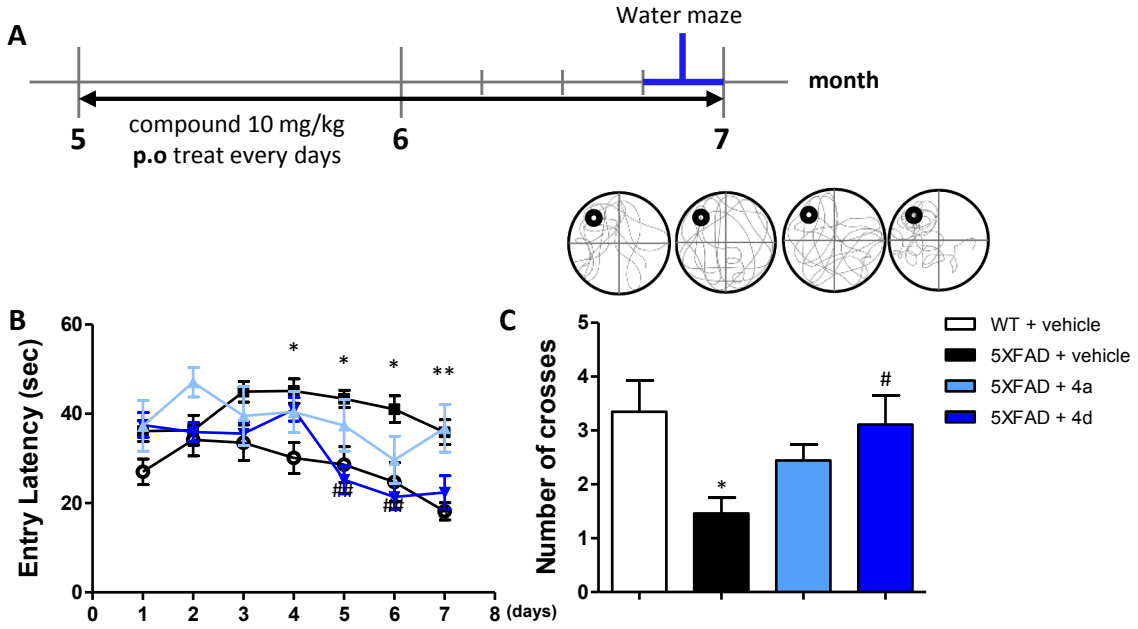

Fig. 7. In vivo effects of polyhydroxyisoflavones in 5XFAD mice. (A) In vivo experimental schedule. (B) Escape latency of wild-type or 5XFAD mice treated with polyhydroxyisoflavones (n = 9–13 per group). (C) The representative swimming path and number of platform crossings in the probe test (n = 9–13 per group). Data are shown as the mean ± SEM. One-way ANOVA. $^{*}P < 0.05$ and $^{**}P < 0.01$ vs. saline-treated wild-type (WT) mice. $^{\#}P < 0.05$ and $^{\#\#}P < 0.01$ vs. saline-treated 5XFAD mice.

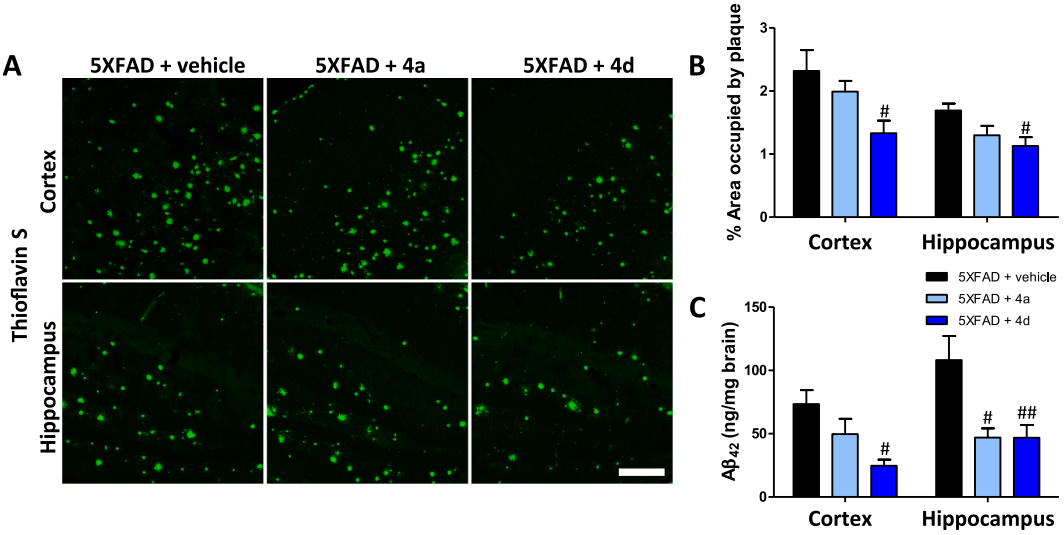

Fig. 8. Representative confocal microscopy images (A) and quantification data (B) of mouse brain slices stained with thioflavin S (n = 4–6 per group, scale bar, 200 μm). (C) Measurement of $A\beta_{42}$ protein levels using an ELISA kit (n = 4–6 per group). Data are shown as the mean ± SEM. One-way ANOVA. $^{\#}P < 0.05$ and $^{\#\#}P < 0.01$ vs. saline-treated 5XFAD mice.

groups, suggesting that our polyhydroxyisoflavones did not affect motor function (Fig. S8). Next, the effect of **4d** on Aβ aggregation was investigated by observing aggregated proteins, including amyloid plaques, in the cortex and hippocampus of 5XFAD mice. As shown in Fig. 8A and 8B, thioflavin S-positive Aβ plaques were observed in 7-month-old 5XFAD mice. However, thioflavin S-positive Aβ plaques were significantly decreased in both the cortex and hippocampus regions of **4d**-treated 5XFAD mice (Fig. 8A and 8B). In the **4a**-treated 5XFAD mice, thioflavin S-positive Aβ plaques were slightly reduced, but the difference did not reach statistical significance (Fig. 8A and 8B). The anti-Aβ aggregation effect of **4d** was further confirmed by human $A\beta_{42}$ ELISA (Fig. 8C).

Immunostaining using a 6E10 antibody showed similar results, supporting the reduction of Aβ plaques by **4d** (Fig. 9). Activation of glial cells, including astrocytes and microglia, is also considered to contribute to AD pathology. In our experiments, the levels of gliosis induced by astrocytes and microglia were increased in 5XFAD mice compared to WT mice, as expected, but these levels did not change after **4d** treatment, indicating that **4d** acts directly on Aβ and tau without glial cell changes (Fig. 10 and Fig. 11). Collectively, our observations and data reveal that **4d** treatment attenuates Aβ aggregation and improves memory deficits in 5XFAD mice.

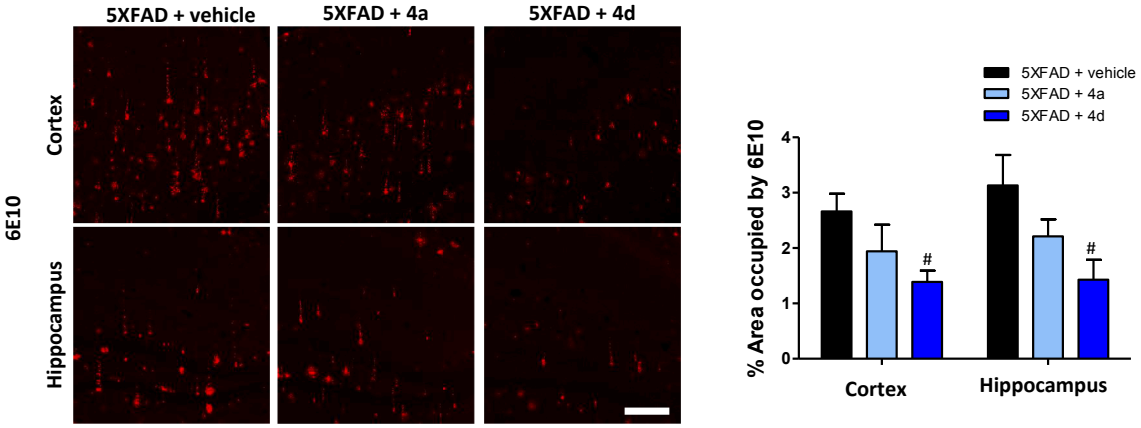

Fig. 9. Representative confocal microscopy images and quantification data of mice brain slices stained with 6E10 antibody (scale bar = 200 μm, n = 4–6 per group). Data are shown as mean ± SEM. One-way ANOVA. $^{\#}P < 0.05$ vs. saline-treated 5XFAD mice.

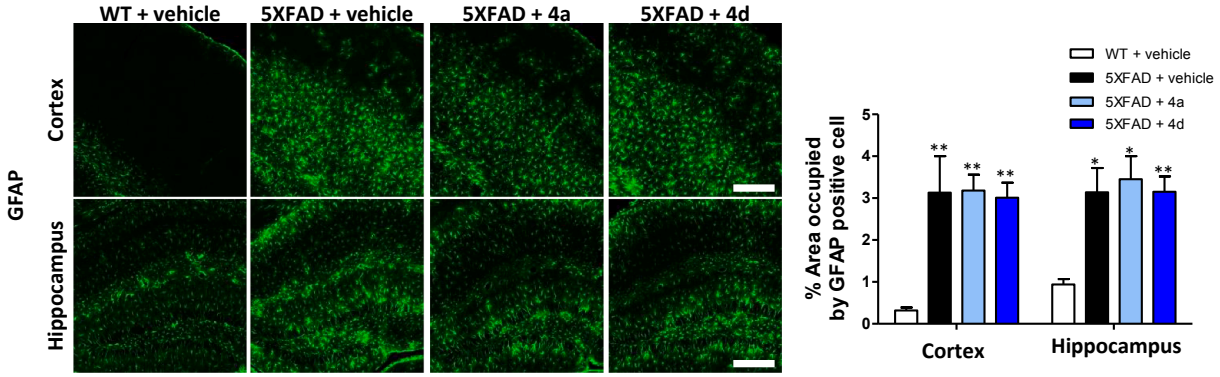

Fig. 10. Representative confocal microscopy images and quantification data of glial activation in the mice brain. (B) Immunofluorescence images and quantification of GFAP (scale bar = 200 μm, n = 4–5 per group). Data are shown as mean ± SEM. One-way ANOVA. $^{*}P < 0.05$ and $^{**}P < 0.01$ vs. saline-treated WT mice.

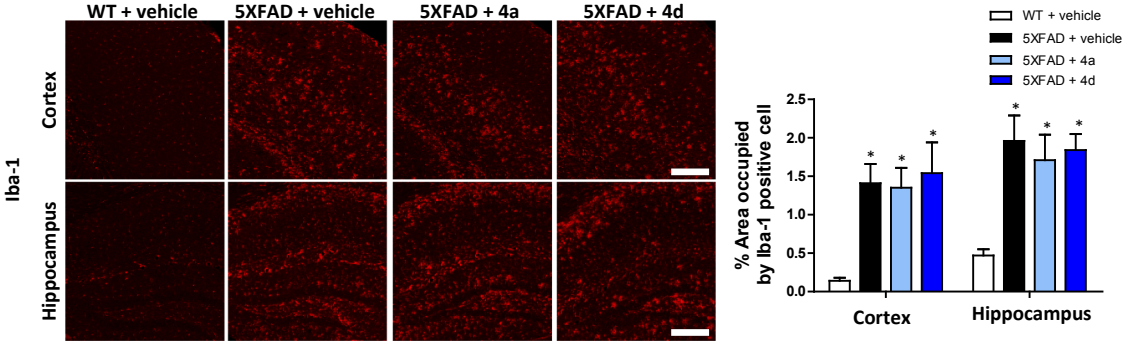

Fig. 11. Representative confocal microscopy images and quantification data of glial activation in the mice brain. Immunofluorescence images and quantification of Iba-1 (scale bar = 200 μm, n = 4–5 per group). Data are shown as mean ± SEM. One-way ANOVA. $^{*}P < 0.05$ vs. saline-treated WT mice.

3. Conclusion

A series of polyhydroxyisoflavones were expediently synthesized and evaluated biologically. An in vitro ThT assay and TEM analysis demonstrated that *ortho*-catechol containing isoflavones were identified as a privileged scaffold that directly prevents the aggregation of both Aβ and tau. By utilizing ^{1}H-^{15}N HSQC spectra, we investigated the mode of action of the catechol-containing isoflavone, **4d**, during the protein aggregation process. Finally, **4d** was shown to alleviate cognitive impairment and pathologies related to AD in a 5XFAD transgenic mouse model.

4. Experimental section

4.1. Chemistry

Unless stated otherwise, all chemicals were obtained from commercial suppliers (Sigma Aldrich, TCI, Alfa Aesar and Acros Organics) and used as received. All reactions were performed under argon atmosphere. ^{1}H NMR was measured and obtained using a Bruker 400 and ^{13}C NMR spectra was measured on a Varian VNMRS500 spectrometer. ^{1}H and ^{13}C NMR chemical shifts were determined relative to the signal of the residual solvent peak used as an internal reference. Signals are

recorded as follows: chemical shift (δ, ppm), multiplicity (s = singlet, d = doublet, t = triplet, m = multiplet, br = broad). Coupling constants (J) were reported in Hertz (Hz). High-resolution mass spectrometry (HRMS) data were recorded using a JEOL JMS-700 instrument in the EI or ESI mode. Flash column chromatography was performed using silica gel 60 (230-400mesh) and analytical thin layer chromatography (TLC) was performed using TLC Silica gel 60 F254. Optical Spectral were measured by NanoDrop One UV/VIS Spectrophotometer (Thermo Fisher Scientific).

4.1.1. General procedure for the preparation of compounds *6a* and *6b*

To a solution of the corresponding hydroxychromone(0.5 mmol, 1 equiv) in dry CH_2Cl_2 (3 mL) was added triethylamine (1.5–2.5 equiv), acetyl chloride (1.5–2.5 equiv) and a catalytic amount of 4-DMAP under argon atmosphere. The resulting solution was stirred at room temperature for the appropriate time. After the reaction was complete, the solution was then diluted with CH_2Cl_2 and quenched with 2 N aqueous HCl solution. The organic phase was combined and dried with anhydrous $MgSO_4$. The solution was filtered and evaporated under reduced pressure. The residue was purified by silica gel flash column chromatography.

*4.1.1.1. 4-oxo-4H-chromen-7-yl acetate **6a**.* **6a** was prepared from 7-hydroxy-4*H*-chromen-4-one (100 mg, 0.617 mmol) using the general procedure described above. Purification by chromatography on silica gel afforded **6a** as a white solid (99 mg, 79% yield); ^{1}H NMR ($CDCl_3$, 400 MHz): δ 8.23 (d, 1H, J = 8.8 Hz), 8.39 (d, 1H, J = 6.1 Hz), 7.28 (d, 1H, J = 2.2 Hz), 7.16 (dd, 1H, J = 8.7, 2.1 Hz), 6.34 (d, 1H, J = 6.0 Hz), 2.34 (s, 3H); ^{13}C NMR ($CDCl_3$, 125 MHz): δ 176.99, 168.67, 157.04, 155.61, 154.62, 127.36, 122.75, 119.67, 113.21, 111.24, 21.26; HR-MS: (EI +) calcd for $C_{11}H_8O_4$, 204.0423; found, 204.0422.

*4.1.1.2. 4-oxo-4H-chromene-5,7-diyl diacetate **6b**.* **6b** was prepared from 5,7-dihydroxy-4*H*-chromen-4-one (300 mg, 1.684 mmol) using the general procedure described above. Purification by chromatography on silica gel afforded **6b** as a white solid (408 mg, 92% yield); ^{1}H NMR ($CDCl_3$, 400 MHz): δ 7.75 (d, 1H, J = 5.9 Hz), 7.22 (d, 1H, J = 2.3 Hz), 6.84 (d, 1H, J = 2.2 Hz), 6.21 (d, 1H, J = 6.0 Hz), 2.42 (s, 3H), 2.34 (s, 3H); ^{13}C NMR ($CDCl_3$, 125 MHz): δ 175.87, 169.61, 168.10, 158.01, 154.48, 154.04, 150.30, 115.98, 114.15, 113.98, 109.26, 21.27, 21.16; HR-MS: (EI +) calcd for $C_{13}H_{11}O_6$, 263.0556; found, 263.0557.

4.1.2. General procedure for the preparation of *1a* and *1b*

To a solution of the corresponding acetoxychromones (0.5 mmol, 1 equiv) and potassium acetate (4 equiv) in AcOH (1.5 mL) was added *N*-bromosuccinimide (1.2 equiv) slowly under argon atmosphere. The reaction mixture was stirred at room temperature for the appropriate time. After the reaction, the solution was diluted with EtOAc and carried out aqueous workup. The organic phase was combined and dried with anhydrous $MgSO_4$. The solvent was filtered and evaporated under reduced pressure. The residue was purified by silica gel flash column chromatography.

*4.1.2.1. 3-bromo-4-oxo-4H-chromen-7-yl acetate **1a**.* **1a** was prepared from **6a** (484 mg, 2.37 mmol) using the general procedure described above. Purification by chromatography on silica gel afforded **1a** as a white solid (166 mg, 25% yield); ^{1}H NMR ($CDCl_3$, 400 MHz): δ 8.29 (d, 1H, J = 8.8 Hz), 8.22 (s, 1H), 7.32 (d, 1H, J = 2.1 Hz), 7.21 (dd, 1H, J = 8.8, 2.1 Hz), 2.36 (s, 3H); ^{13}C NMR (DMSO-d_6, 125 MHz): δ 171.38, 169.17, 156.67, 156.40, 155.28, 127.47, 121.44, 120.83, 112.27, 110.13, 21.44; HR-MS: (EI +) calcd for $C_{11}H_7BrO_4$, 281.9528; found, 281.9526.

*4.1.2.2. 3-bromo-4-oxo-4H-chromene-5,7-diyl diacetate **1b**.* **1b** was prepared from **6b** (360 mg, 1.374 mmol) using the general procedure described above. Purification by chromatography on silica gel afforded **1b** as a colorless oil (149 mg, 32% yield (79% yield brsm)); ^{1}H NMR ($CDCl_3$, 400 MHz): δ 7.75 (d, 1H, J = 5.9 Hz), 7.22 (d, 1H, J = 2.3 Hz), 6.84 (d, 1H, J = 2.2 Hz), 6.21 (d, 1H, J = 6.0 Hz), 2.42 (s, 3H), 2.34 (s, 3H); ^{13}C NMR (DMSO-d_6, 125 MHz): δ 169.97, 169.41, 168.87, 157.58, 155.52, 154.75, 149.98, 115.55, 114.41, 110.92, 110.35, 21.41, 21.32; HR-MS: (EI +) calcd for $C_{13}H_{10}BrO_6$, 340.9661; found, 340.9662.

4.1.3. General procedure for the preparation of *3a-3g*

3-Bromochromone (0.5 mmol, 1 equiv), benzeneboronic acid (1.5 equiv), palladium acetate (0.3 equiv), potassium carbonate (4 equiv) and SPhos (0.5 equiv) were added in a round-bottomed flask. DMF/H_2O (3:1, 5 mL) was added under argon atmosphere. The reaction was stirred at 90 °C under argon atmosphere until completion of the reaction. After cooling, the solution was quenched with 2 N aqueous HCl solution and extracted by EtOAc. The organic phase was combined and dried with anhydrous Na_2SO_4, and then filtered. The filtrate was evaporated under reduced pressure and purified by silica gel flash column chromatography.

*4.1.3.1. 7-hydroxy-3-(4-methoxyphenyl)-4H-chromen-4-one **3a**.* **3a** was prepared from **1a** (50 mg, 0.177 mmol) and (4-methoxyphenyl)boronic acid (40 mg, 0.263 mmol) using the general procedure described above. Purification by chromatography on silica gel afforded **3a** as a white solid (25 mg, 53%); ^{1}H NMR (DMSO-d_6, 400 MHz): δ 8.33 (s, 1H), 7.97 (d, 1H, J = 8.8 Hz), 7.51 (d, 2H, J = 8.7 Hz), 6.99 (d, 2H, J = 8.8 Hz), 6.93 (d, 1H, J = 8.8 Hz), 6.86 (s, 1H), 3.79 (s, 3H).

*4.1.3.2. 5,7-dihydroxy-3-(4-methoxyphenyl)-4H-chromen-4-one **3b**.* **3b** was prepared from **1b** (190 mg, 0.559 mmol) and (4-methoxyphenyl) boronic acid (127 mg, 0.836 mmol) using the general procedure described above. Purification by chromatography on silica gel afforded **3b** as a pale yellow solid (29 mg, 18%); ^{1}H NMR ($CDCl_3$, 400 MHz): δ 12.93 (s, 1H), 7.86 (s, 1H), 7.46 (d, 2H, J = 8.9 Hz), 6.98 (d, 2H, J = 8.8 Hz), 6.37 (d, 1H, J = 2.3 Hz), 6.30 (d, 1H, J = 2.1 Hz) 3.85 (s, 3H).

*4.1.3.3. 3-(3,4-dimethoxyphenyl)-7-hydroxy-4H-chromen-4-one **3c**.* **3c** was prepared from **1a** (98 mg, 0.346 mmol) and (3,4-dimethoxyphenyl) boronic acid (95 mg, 0.522 mmol) using the general procedure described above. Purification by chromatography on silica gel afforded **3c** as a white solid (41 mg, 40%); ^{1}H NMR (DMSO-d_6, 400 MHz): δ 8.37 (s, 1H), 7.97 (d, 1H, J = 8.7 Hz), 7.19 (s, 1H), 7.12 (dd, 1H, J = 8.3, 1.9 Hz), 7.0 (d, 1H, J = 8.3 Hz), 6.94 (dd, 1H, J = 8.8, 2.3 Hz), 6.87 (d, 1H, J = 2.0 Hz) 3.78 (s, 6H).

*4.1.3.4. 3-(3,4-dimethoxyphenyl)-5,7-dihydroxy-4H-chromen-4-one **3d**.* **3d** was prepared from **1b** (156 mg, 0.459 mmol) and (3,4-dimethoxyphenyl)boronic acid (125 mg, 0.687 mmol) using the general procedure described above. Purification by chromatography on silica gel afforded **3d** as a white solid (87 mg, 60%); ^{1}H NMR (DMSO-d_6, 400 MHz): δ 12.95 (s, 1H), 10.90 (s, 1H), 8.41 (s, 1H), 7.17 (s, 1H), 7.12 (d, 1H, J = 8.1 Hz), 7.02 (d, 1H, J = 8.2 Hz), 6.40 (s, 1H), 6.24 (s, 1H), 3.78 (s, 6H).

*4.1.3.5. 3-(3,4-dimethoxyphenyl)-4H-chromen-4-one **3e**.* **3e** was prepared from commercially available 3-bromo-4*H*-chromen-4-one (100 mg, 0.444 mmol) and (3,4-dimethoxyphenyl)boronic acid (121 mg, 0.665 mmol) using the general procedure described above. Purification by chromatography on silica gel afforded 3e as a white solid (89 mg, 71%); ^{1}H NMR ($CDCl_3$, 400 MHz): δ 8.32 (dd, 1H, J = 8.0, 1.6 Hz), 8.03 (s, 1H), 7.69 (m, 1H), 7.49 (d, 1H, J = 8.5 Hz), 7.44 (m, 1H), 7.22 (d, 1H, J = 2.0 Hz), 7.07 (dd, 1H, J = 8.2, 2.0 Hz), 6.94 (d, 1H, J = 8.3 Hz), 3.94 (s, 3H), 3.92 (s, 3H).

*4.1.3.6. 5,7-dihydroxy-3-phenyl-4H-chromen-4-one **3f**.* **3f** was prepared

from **1b** (48 mg, 0.141 mmol) and phenylboronic acid (26 mg, 0.213 mmol) using the general procedure described above. Purification by chromatography on silica gel afforded **3f** as a pale yellow solid (13 mg, 36%); ^{1}H NMR (DMSO-d_6, 400 MHz): δ 12.89 (s, 1H), 10.97 (s, 1H), 8.44 (s, 1H), 7.56 (m, 2H), 7.45 (m, 3H), 6.42 (s, 1H), 6.24 (s, 1H); ^{13}C NMR (DMSO-d_6, 125 MHz): δ 180.45, 165.00, 162.54, 158.14, 155.55, 131.38, 129.54, 128.77, 128.58, 122.84, 104.99, 99.66, 94.34; HR-MS: (EI +) calcd for $C_{15}H_{10}O_4$, 254.0579; found, 254.0573.

*4.1.3.7. 3-phenyl-4H-chromen-4-one **3g**.* **3 g** was prepared from 3-bromo-4*H*-chromen-4-one **1c** (100 mg, 0.444 mmol) and phenylboronic acid (81 mg, 0.664 mmol) using the general procedure C described above. Purification by chromatography on silica gel afforded **3 g** as a white solid (85 mg, 86%); ^{1}H NMR ($CDCl_3$, 400 MHz): δ 8.32 (dd, 1H, J = 8.0, 1.6 Hz), 7.69 (m, 1H), 7.58 (m, 2H), 7.51–7.38 (m, 5H); ^{13}C NMR ($CDCl_3$, 125 MHz): δ 176.36, 156.30, 153.21, 133.75, 131.94, 129.07, 128.63, 128.32, 126.53, 125.49, 125.37, 124.67, 118.17; HR-MS: (EI +) calcd for $C_{15}H_{10}O_2$, 222.0681; found, 222.0684.

4.1.4. General procedure for the preparation of **4a**-**4e**

Mixture of corresponding isoflavone (0.1 mmol) and pyridine hydrochloride (1.34 g) in a round-bottomed flask was heated and stirred at 150 °C for the appropriate time. After the reaction was completed, the solution was cooled and poured into 2 *N* aqueous HCl solution. After aqueous workup, extraction with EtOAc was performed and dried with Na_2SO_4. The solution was filtered and evaporated under reduced pressure. The residue was purified by flash chromatography on silica gel.

*4.1.4.1. 7-hydroxy-3-(4-hydroxyphenyl)-4H-chromen-4-one **4a**.* **4a** was prepared from **3a** (20 mg, 0.075 mmol) using the general procedure described above. Purification by chromatography on silica gel afforded daidzein **4a** as a white solid (7.2 mg, 38%); All spectroscopic data were consistent with previously reported data [51].

*4.1.4.2. 5,7-dihydroxy-3-(4-hydroxyphenyl)-4H-chromen-4-one **4b**.* **4b** was prepared from **3b** (23 mg, 0.082 mmol) using the general procedure described above. Purification by chromatography on silica gel afforded **4b** as a pale yellow solid (12.5 mg, 56%); ^{1}H NMR (DMSO-d_6, 400 MHz): δ 12.96 (s, 1H), 8.33 (s, 1H), 7.38 (d, 2H, J = 8.5 Hz), 6.82 (d, 2H, J = 8.6 Hz), 6.39 (d, 1H, J = 2.0 Hz), 6.22 (d, 1H, J = 2.0 Hz); ^{13}C NMR (DMSO-d_6, 125 MHz): δ 180.76, 164.83, 162.53, 158.12, 157.95, 154.55, 130.71, 122.80, 121.73, 115.59, 104.98, 99.50, 94.20; HR-MS: (EI +) calcd for $C_{15}H_{10}O_5$, 270.0528; found, 270.0526.

*4.1.4.3. 3-(3,4-dihydroxyphenyl)-7-hydroxy-4H-chromen-4-one **4c**.* **4c** was prepared from **3c** (32 mg, 0.107 mmol) using the general procedure described above. Purification by chromatography on silica gel afforded **4c** as a pale yellow solid (4.2 mg, 15%); ^{1}H NMR (DMSO-d_6, 400 MHz): δ 10.80 (bs, 1H), 8.99 (bs, 2H), 8.26 (s, 1H), 7.96 (d, 1H, J = 8.7 Hz), 7.02 (s, 1H), 6.93 (d, 1H, J = 8.6 Hz), 6.86 (s, 1H), 6.78 (m, 2H); ^{13}C NMR (DMSO-d_6, 125 MHz): δ 175.21, 163.00, 157.89, 153.34, 145.79, 145.31, 127.85, 124.14, 123.51, 120.36, 117.18, 117.12, 115.81, 115.63, 102.61; HR-MS: (EI +) calcd for $C_{15}H_{10}O_5$, 270.0528; found, 270.0527.

*4.1.4.4. 3-(3,4-dihydroxyphenyl)-5,7-dihydroxy-4H-chromen-4-one **4d**.* **4d** was prepared from **3d** (65 mg, 0.227 mmol) using the general procedure described above. Purification by chromatography on silica gel afforded **4d** as a pale yellow solid (45.6 mg, 70%); ^{1}H NMR (DMSO-d_6, 400 MHz): δ 13.00 (s, 1H), 10.88 (s, 1H), 9.08 (s, 1H), 9.01 (s, 1H), 8.29 (s, 1H), 6.99 (s, 1H), 6.78 (m, 2H), 6.38 (s, 1H), 6.22 (s, 1H); ^{13}C NMR (DMSO-d_6, 125 MHz): δ 180.78, 164.77, 162.55, 158.07, 154.49, 146.06, 145.43, 122.94, 122.16, 120.49, 117.07, 115.91, 105.00, 99.47, 94.16; HR-MS: (EI +) calcd for $C_{15}H_{10}O_6$, 286.0477; found, 286.0472.

*4.1.4.5. 3-(3,4-dihydroxyphenyl)-4H-chromen-4-one **4e**.* **4e** was prepared from **3e** (75 mg, 0.266 mmol) using the general procedure described above. Purification by chromatography on silica gel afforded **4e** as a yellow solid (30 mg, 44%); ^{1}H NMR (DMSO-d_6, 400 MHz): δ 8.32 (dd, 1H, J = 8.0, 1.6 Hz), 8.04 (s, 1H), 7.71 (m, 1H), 7.51 (d, 1H, J = 8.9 Hz), 7.45 (t, 1H, J = 7.4 Hz), 7.23 (d, 1H, J = 1.7 Hz), 6.89 (m, 2H), 6.72 (s, 1H), 5.81 (s, 1H); ^{13}C NMR (DMSO-d_6, 125 MHz): δ 175.89, 156.08, 154.19, 145.95, 145.39, 134.56, 126.06, 125.92, 124.55, 124.34, 123.25, 120.40, 118.89, 117.08, 115.87; HR-MS: (EI +) calcd for $C_{15}H_{10}O_4$, 254.0579; found, 254.0578.

4.1.5. UV/Vis spectrophotometer analysis

For UV/Vis spectrophotometer investigating the interaction of **4d** with Cu(II), the analysis was conducted in a Chelex-treated HEPES buffer solution (10 mM HEPES, 100 mM NaCl, pH 7.4) [49]. The solution of **4d** (100 μM) was titrated up to 4 equiv of $CuCl_2$ at room temperature. The spectraphotometer anylasis was conducted 5 min after the addtion of $CuCl_2$.

4.2. Biological evaluation

Thioflavin T (ThT), Thioflavin S, anhydrous dimethyl sulfoxide (DMSO), triton X-100, paraformaldehyde, phosphate buffer, phosphate-buffered saline (PBS, pH 7.4), Heparin sodium salt from porcine intestinal mucosa, 1,1,1,3,3,3-hexafluoroisopropanol (HFIP) and Guanidine hydrochloride were purchased from Sigma Aldrich (St. Louis, MO, USA). Fluorescence mounting medium was purchased from Dako (Santa Clara, CA, USA). Chelex was purchased from Bio-rad (Bio-Rad Laboratories, Hercules, CA, USA). Amyloid beta (Aβ) 1–42 peptide was purchased from Anaspec (Fremont, CA, USA).

4.2.1. Aβ peptides preparation

To ensure the monomeric state of the peptide, Aβ peptides were dissolved in HFIP, incubated for 3 days at room temperature. The solvent was then removed by speed vacuum. The monomerized Aβ was stored as powder at −80 °C until use.

4.2.2. Tau purification

Wild-type human tau (2N4R isoform, 441 residues) pET29b plasmid was purchased from Addgene (#16316). The plasmid was transformed into Escherichia coli strain BL21 (DE3) Codon Plus cells. Cells were grown at 37 °C in LB medium containing 50 mg/mL kanamycin until the OD_{600} reached 0.6, then overexpression was induced by adding 0.5 mM isopropyl β-D-thiogalactopyranoside (IPTG), followed by 4 h of incubation at 37 °C. Cells were harvested by centrifugation at 7500*g* for 10 min. Collected pellets were resuspended in lysis buffer (25 mM Tris-HCl pH 6.8, 500 mM NaCl, 1 mM EDTA, 1 mM $MgCl_2$, 5 mM dithiothreitol (DTT)) and disrupted by sonication. The lysates were boiled for 20 min and clarified by centrifugation at 36,000*g* for 45 min and cell debris was removed. The supernatant was diluted to a final salt concentration of 50 mM NaCl, then purified using anion exchange column (HiTrap Q HP, 1 × 5 mL, GE Healthcare Life Sciences) equilibrated with 25 mM Tris-HCl pH 6.8, 50 mM NaCl, 1 mM EDTA, 1 mM $MgCl_2$, 2 mM DTT, 0.2 mM phenylmethylsulfonyl fluoride (PMSF) in an ÄKTAprime plus (GE Healthcare Life Sciences). Bound proteins were eluted with a salt gradient from 50 mM to 1 M NaCl. Further purification was performed using HiLoad 16/600 Superdex 200 prep-grade column in an ÄKTApurifier (GE Healthcare Life Sciences) with PBS buffer. Purified tau protein was concentrated by ultrafiltration (Amicon, 10 kDa cut-off, Millipore) up to 2.6 mg/mL.

4.2.3. Recombinant tau protein preparation

Various human tau cDNA was constructed in a pRK172 vector based on the longest form of human wild-type tau encoded 441 amino acid (2N4R); deletion of amino acids at positions 252 to 376 (DMTBR), positions 306 to 311 (DPHF6), positions 275 to 280 (DPHF6*) and with

substitutions at C291A and C322A (C291, 322A). A construct that encoded 2N3R tau with a mutation at C322A (2N3R-C322A) was produced. Each recombinant tau was expressed in Escherichia coli BL21 (DE3) and purified by modified method reported previously. After E. coli expressing tau was sonicated and boiled, recombinant tau proteins in the heat-stable fraction was purified by ion-exchange chromatography (P11; GE Healthcare, or Cellufine Phosphate; JNC Corp.), ammonium sulfate fractionation, gel filtration chromatography (NAP10 column; GE Healthcare) and reverse phase-HPLC (COSMOSIL Protein-R Waters; Nacalai Tesque Inc.). After freeze-drying, recombinant tau proteins were dissolved in milliQ water and stored at −80 °C as a stock solution.

4.2.4. ThT fluorescence assay

The ThT binding activity of some compounds was determined in black 96-well flat-bottom plates. For Aβ ThT assays examining the effect of compounds on aggregation, Aβ (10 μM) was incubated in the absence or presence of $CuCl_2$ or $ZnCl_2$ (10 μM) and compounds (30 μM) in a HEPES solution (20 mM, 150 mM NaCl, pH 7.4) containing ThT (20 μM) [52]. The plates were incubated at 37 °C without shaking. At specific time points, fluorescence generated by the binding of ThT to Aβ aggregates was measured using a plate reader (FLUOstar Omega, BMG labtech, Ortenberg, Germany) at excitation and emission wavelengths of 430 and 492 nm, respectively [26,65]. For Tau ThT assays examining the effect of compounds on aggregation, Recombinant wild-type 2N4R tau (10 μM), compounds (30 μM) and ThT (20 μM) were mixed in the a HEPES solution (10 mM, 100 mM NaCl, pH 7.4), and incubated with heparin (0.06 mg/mL) at 37 °C without shaking. At specific time points, fluorescence generated by the binding of ThT to tau aggregates was measured using a plate reader at excitation and emission wavelengths of 430 and 492 nm, respectively [51]. When primary inner filter effect (IFE) might be necessary to be mainly considered in the reaction condition, we applied a below equation to our experimental results, following Beer-Lambert's law [66,67].

$$F_{corr} = F_{obs}\exp[(A_{exc} + A_{em}) / 2]$$

4.2.5. Transmission electron microscopy (TEM)

Monomerized Aβ were dissolved in HEPES buffer (20 mM, 150 mM NaCl, pH 7.4) to a final protein concentration of 10 μM and incubated in the absence or presence compounds (30 μM) at 37 °C for 24 h without agitation [42]. For Tau ThT assays examining the effect of compounds on aggregation, recombinant wild-type 2N4R tau (10 μM), compounds (30 μM) were mixed in the a HEPES solution (10 mM, 100 mM NaCl, pH 7.4), and incubated with heparin (0.06 mg/mL) at 37 °C without shaking [51].

Samples were prepared for TEM studies by spotting aliquots (5 μL) of the aggregation assay onto 200 mesh Carbon coated Cupper grid (SPI supplies, West Chester, PA). The samples were then blotted with a filter paper and allowed to dry. The dried samples were negatively stained with 2% uranyl acetate in water (5 μL) for 30 s, washed with water, blotted with a filter paper, and dried again. Samples were then analyzed by a Tecnai G2 F20 TEM (FEI Tecnai™ G2, Hillsboro, Oregon) operated at 200 kV [42,68].

4.2.6. NMR experiments

For NMR titration of **4d** to $A\beta_{42}$, uniformly ^{15}N-labeled $A\beta_{42}$ peptide was purchased from rPeptide (A-1102–2). 100 μL of 1% NH_4OH was added to 1 mg of the lyophilized ^{15}N-labeled $A\beta_{42}$ powder, and the solution was diluted with NMR buffer (20 mM Tris-HCl pH 7.4, 50 mM NaCl and 10% D_2O). 50 μM ^{15}N-labeled $A\beta_{42}$ in NMR buffer was titrated by 3 (150 μM), 6 (300 μM), 9 (450 μM) and 12 (600 μM) molar equivalents of **4d**. The 2D ^{1}H-^{15}N heteronuclear single quantum correlation (HSQC) spectra were measured at 5 °C with 16 scans per increment and 2048 X 128 points in the ^{1}H and ^{15}N dimensions, respectively.

Fibrillation of $A\beta_{42}$ was accelerated by shaking the samples with 200 rpm at 25 °C without addition of an agent. The ^{15}N-labeled $A\beta_{42}$ (25 μM) in the presence or absence of **4d** (100 μM) were incubated with shaking for 4 h and 12 h, respectively. After incubation, the 2D ^{1}H-^{15}N HSQC spectra of $A\beta_{42}$ were obtained at 5 °C.

For NMR titration of **4d** to tau, uniformly ^{15}N-labeled tau was prepared by growing the cells in M9 minimal medium containing 1 g/L $^{15}NH_4Cl$. The ^{15}N-labeled tau was expressed and purified as described above. Final NMR samples were dissolved in a buffer containing 50 mM sodium phosphate pH 6.4, 50 mM NaCl, 2.5 mM DTT, 2.5 mM EDTA, 3% d6-dimethyl sulfoxide (DMSO) and 10% D_2O. **4d** was added to the 50 μM ^{15}N-labeled tau with molar ratios of 1:2 (100 μM), 1:4 (200 μM), 1:6 (300 μM) and 1:12 (600 μM). The 2D ^{1}H-^{15}N HSQC spectra were collected at 20 °C with 8 scans per increment and 1024 X 256 points in the ^{1}H and ^{15}N dimensions, respectively.

To induce the fibrillation of tau, 0.3 mg/mL of heparin was added to 50 μM ^{15}N-labeled tau in the presence or absence of 200 μM of **4d**, respectively. NMR measurement was started immediately after addition of heparin. The 2D ^{1}H-^{15}N HSQC experiments of ^{15}N-labeled tau were recorded at 37 °C. The HSQC spectra of ^{15}N-labeled tau in the presence or absence of **4d** were acquired consecutively for 21 h. All NMR spectra were measured on a Bruker AVANCE III 800-MHz spectrometer equipped with a cryogenic probe, and NMR data were processed using NMRPipe and NMRDraw software, and spectrum analysis was performed by NMRView *J* program.

4.2.7. Animals and treatment

5XFAD mice were purchased from Jackson Laboratory (stock number: 034840-JAX, Bar Harbor, ME, USA). Mice were housed in plastic containers under constant temperature (23 ± 1 °C) and humidity (60 ± 10%), in a 12-h light/dark cycle with free access to food and water. 5XFAD transgenic mice overexpress human APP695 with three familial mutations (Swedish [K670N, M671L], Florida [I716V] and London [V717I]) and human presenilin 1 with two familial mutations (M146L and L286V) under the control of the murine Thy1 promotor (Moechars, Lorent, De Strooper, Dewachter, & Van Leuven, 1996). Five-month-old 5XFAD female mice (22 ± 2 g) and male mice (30 ± 2 g) were injected intraperitoneally with 10 mg/kg of compound in saline (0.9% NaCl) per day for eight weeks. All animal studies were performed in accordance with the "Principles of Laboratory Animal Care" (National Institutes of Health publication number 80–23, revised 1996) and approved by the Animal Care and Use Guidelines Committee of Kyung Hee University (approval number: KHUASP(SE)-17–126-1).

4.2.8. Morris water maze

Morris water maze (MWM) task was used to assess spatial memory performance. The water maze was a white tank (1.0 m in diameter, 40 cm in height) filled to a depth of 30 cm with water (22–24 °C). White, opaque, nontoxic paint was used to hinder visibility. A submerged plexiglas platform (10 cm in diameter, placed 6–8 mm below the surface of the water) was located at a fixed position throughout the training session. The position of the platform varied from mouse to mouse while being counterbalanced across experiment groups. All mice were habituated to the maze one day before training. The training session consisted of a series of three trials per day for seven consecutive days, for a total of 21 trials. In each of the three trials, the animals were placed at different starting positions that were equally spaced around the perimeter of the pool in a random order. The mouse was given 60 *sec* to find the submerged platform. If the mouse did not mount the platform within 60 *sec*, it was guided to the platform. The time to mount the platform was recorded as latency for each trial. Mice were allowed to remain on the platform for 10 *sec* before being returned to a home cage. On the eight day, a single probe trial, in which the platform was removed, was performed after the hidden platform task was completed. Each mouse was placed into one quadrant of the pool and allowed to swim for 60 *sec*. All trials were recorded using a charge-coupled device camera connected to

a video monitor and a computer and analyzed by the free tracking software tool Toxtrac (Rodriguez, Zhang, Klaminder, Brodin, & Andersson, 2017). The software, user manual, and documentation are available at https://toxtrac.sourceforge.io. The operators responsible for experimental procedure and data analysis were blinded and unaware of group allocation throughout the experiments

4.2.9. Brain tissue preparation

Mice were euthanized after behavioral testing by administration of a mixture of ketamine and xylazine in saline (0.9% NaCl) as the anesthetic, and cardiac perfusion was performed immediately using 4% paraformaldehyde in PBS. After perfusion, brains were removed, post-fixed overnight at 4 °C, and incubated in 30% sucrose at 4 °C until equilibration. Sequential 30-μm-thick coronal sections were prepared by a cryostat (CM1850; Leica, Wetzlar, Germany) and stored at −20 °C.

4.2.10. Thioflavin s staining

Free-floating sections were incubated for 10 min in 1% thioflavin S dissolved in 50% ethanol, followed by two washes with 50% ethanol for 5 min each and one wash with tap water for 5 min; the sections were then mounted using mounting medium.

4.2.11. Immunofluorescence

Free-floating sections were incubated for 1 h in PBS containing 3% normal goat serum, 1% bovine serum albumin (BSA), and 0.4% triton X-100. In the same buffer solution, the sections were then incubated for 24 h in primary antibodies at 4 °C. The following antibodies were used: 6E10 (Biolegend, #803001), GFAP (Dako, #Z0334) and Iba-1 (Wako Chemical, #019-19741). For visualization, the sections were incubated with Alexa Fluor 488- or 594-conjugated secondary antibodies for 1 h at room temperature. Images of the sections were captured using laser-scanning confocal microscopy (K1-Fluo; Nanoscope Systems, Daejeon, Republic of Korea) or a BX51 immunofluorescence microscope (Olympus, Tokyo, Japan). Image *J* software was used for quantification.

4.2.12. Aβ 1–42 enzyme-linked immunosorbent assays

Aβ 1–42 enzyme-linked immunosorbent assays (ELISAs) were performed using fluorescent-based ELISA kit (Invitrogen, Camarillo, CA, USA) and appropriate Aβ standards according to the manufacturer's protocol. In each mouse, the hippocampus and frontal cortex from one hemisphere were homogenized in guanidine buffer containing 50 mM Tris and 5 M guanidine HCl (pH 8.0). Homogenates were mixed at room temperature for 4 h and diluted in PBS containing 5% BSA, 0.03% tween 20, and protease inhibitor cocktail (Calbiochem, San Diego, CA, USA). All Aβ standards and experimental samples were run in duplicates, and the results were averaged.

4.2.13. Statistical analysis

The results from three independent experiments were summarized and presented as means ± standard error of the mean (S.E.M.). Statistical comparisons between each group were performed with a one-way analysis of variance followed by Tukey's multiple comparison post hoc test, and p values less than 0.05 were considered to indicate statistically significant differences from the controls, as indicated by an asterisk. The GraphPad Prism 5.0 software (Graph Pad Software, San Diego, CA, USA) was used for all statistical analyses.

4.2.14. LC/MS

A cysteine or *N*-acetyl cysteine (10 μM) was incubated with compound **4d** (100 μM) in the HEPES buffer (10 mM HEPES, pH = 7.4; 100 mM NaCl) for 5 days at 37 °C [48]. After incubation, the samples were diluted and analyzed using ACQUITY UPLC H-Class PLUS with QDA system (Waters). Mass spectrometric analysis was performed in the positive and negative electrospray mode using a spray voltage of 1.3 kV, 15CV and a capillary temperature of 300 °C with nitrogen as the sheath and auxiliary gas.

Declaration of Competing Interest

The author declare that there is no conflict of interest.

Acknowledgments

This work was supported by the National Research Foundation of Korea (NRF) grant funded by the Korea government (MSIT) (NRF-2020R1F1A1064755 and 2020R1A2C300888911).

Appendix A. Supplementary material

Supplementary data to this article can be found online at https://doi.org/10.1016/j.bioorg.2021.105022.

References

[1] P. Scheltens, K. Blennow, M.M.B. Breteler, B. de Strooper, G.B. Frisoni, S. Salloway, W.M. Van der Flier, Alzheimer's disease, Lancet 388 (2016) 505–517.
[2] A. Abbott, Dementia: a problem for our age, Nature 475 (2011) S2–S4.
[3] G. Livingston, J. Huntley, A. Sommerlad, D. Ames, C. Ballard, S. Banerjee, C. Brayne, A. Burns, J. Cohen-Mansfield, C. Cooper, S.G. Costafreda, A. Dias, N. Fox, L.N. Gitlin, R. Howard, H.C. Kales, M. Kivimäki, E.B. Larson, A. Ogunniyi, V. Orgeta, K. Ritchie, K. Rockwood, E.L. Sampson, Q. Samus, L.S. Schneider, G. Selbæk, L. Teri, N. Mukadam, Dementia prevention, intervention, and care, report of the Lancet Commission, Lancet 396 (2020) (2020) 413–446.
[4] M. Piton, C. Hirtz, C. Desmetz, J. Milhau, A.D. Lajoix, K. Bennys, S. Lehmann, A. Gabelle, Alzheimer's disease: advances in drug development, J. Alzheimers Dis. 65 (2018) 3–13.
[5] J. Cummings, G. Lee, A. Ritter, K. Zhong, Alzheimer's disease drug development pipeline: 2018, Alzheimer's Dementia 4 (2018) 195–214.
[6] I.W. Hamley, The amyloid beta peptide: a chemist's perspective. Role in Alzheimer's and Fibrillization, Chem. Rev. 112 (2012) 5147–5192.
[7] C.L. Masters, R. Bateman, K. Blennow, C.C. Rowe, R.A. Sperling, J.L. Cummings, Alzheimer's disease, Nat. Rev. Dis. Primers 1 (2015) 15056.
[8] M. Goedert, M.G. Spillantini, A century of Alzheimer's disease, Science 314 (2006) 777–781.
[9] P.V. Arriagada, J.H. Growdon, E.T. Hedley-Whyte, B.T. Hyman, Neurofibrillary tangles but not senile plaques parallel duration and severity of Alzheimer's disease, Neurology 42 (1992) 631–639.
[10] J. Götz, A. Ittner, L.M. Ittner, Tau-targeted treatment strategies in Alzheimer's disease, Br. J. Pharmacol. 165 (2012) 1246–1259.
[11] I. Kolaj, S. Imindu Liyanage, D.F. Weaver, Phenylpropanoids and Alzheimer's disease: A potential therapeutic platform, Neurochem. Int. 120 (2018) 99–111.
[12] L.S. Honig, B. Vellas, M. Woodward, M. Boada, R. Bullock, M. Borrie, K. Hager, N. Andreasen, E. Scarpini, H. Liu-Seifert, M. Case, R.A. Dean, A. Hake, K. Sundell, V. Poole Hoffmann, C. Carlson, R. Khanna, M. Mintun, R. DeMattos, K.J. Selzler, E. Siemers, Trial of solanezumab for mild dementia due to Alzheimer's disease, N. Engl. J. Med. 378 (2018) 321–330.
[13] R. Vandenberghe, J.O. Rinne, M. Boada, S. Katayama, P. Scheltens, B. Vellas, M. Tuchman, A. Gass, J.B. Fiebach, D. Hill, K. Lobello, D. Li, T. McRae, P. Lucas, I. Evans, K. Booth, G. Luscan, B.T. Wyman, L. Hua, L. Yang, H.R. Brashear, R. S. Black, B., for the, I. Clinical Study, Bapineuzumab for mild to moderate Alzheimer's disease in two global, randomized, phase 3 trials, Alzheimer's Res Ther. 8 (2016) 18.
[14] S. Lesné, M.T. Koh, L. Kotilinek, R. Kayed, C.G. Glabe, A. Yang, M. Gallagher, K. H. Ashe, A specific amyloid-β protein assembly in the brain impairs memory, Nature 440 (2006) 352–357.
[15] W.S. Shin, J. Di, Q. Cao, B. Li, P.M. Seidler, K.A. Murray, G. Bitan, L. Jiang, Amyloid β-protein oligomers promote the uptake of tau fibril seeds potentiating intracellular tau aggregation, Alzheimer's Res. Ther. 11 (2019) 86.
[16] T. Wisniewski, F. Goñi, Immunotherapy for Alzheimer's disease, Biochem. Pharmacol. 88 (2014) 499–507.
[17] Y.J. Wang, Alzheimer disease: lessons from immunotherapy for Alzheimer disease, Nat. Rev. Neurol. 10 (2014) 188–189.
[18] Ronald B. DeMattos, J. Lu, Y. Tang, Margaret M. Racke, Cindy A. DeLong, John A. Tzaferis, Justin T. Hole, Beth M. Forster, Peter C. McDonnell, F. Liu, Robert D. Kinley, William H. Jordan, Michael L. Hutton, A Plaque-Specific Antibody Clears Existing β-amyloid Plaques in Alzheimer's Disease Mice, Neuron 76 (2012) 908-920.
[19] R.M. Koffie, M. Meyer-Luehmann, T. Hashimoto, K.W. Adams, M.L. Mielke, M. Garcia-Alloza, K.D. Micheva, S.J. Smith, M.L. Kim, V.M. Lee, B.T. Hyman, T. L. Spires-Jones, Oligomeric amyloid β associates with postsynaptic densities and correlates with excitatory synapse loss near senile plaques, Proc. Natl. Acad. Sci. U. S.A. 106 (2009) 4012–4017.
[20] C.A. Lasagna-Reeves, D.L. Castillo-Carranza, U. Sengupta, M.J. Guerrero-Munoz, T. Kiritoshi, V. Neugebauer, G.R. Jackson, R. Kayed, Alzheimer brain-derived tau oligomers propagate pathology from endogenous tau, Sci. Rep. 2 (2012) 700.
[21] C. Katryna, L.C. Grace, J.H. Carol, K. Jeff, Structure and mechanism of action of tau aggregation inhibitors, Curr. Alzheimer Res. 11 (2014) 918–927.

[22] C.A. Lasagna-Reeves, D.L. Castillo-Carranza, U. Sengupta, A.L. Clos, G.R. Jackson, R. Kayed, Tau oligomers impair memory and induce synaptic and mitochondrial dysfunction in wild-type mice, Mol. Neurodegener. 6 (2011) 39.

[23] N. Bijari, S. Balalaie, V. Akbari, F. Golmohammadi, S. Moradi, H. Adibi, R. Khodarahmi, Effective suppression of the modified PHF6 peptide/1N4R Tau amyloid aggregation by intact curcumin, not its degradation products: another evidence for the pigment as preventive/therapeutic "functional food", Int. J. Biol. Macromol. 120 (2018) 1009–1022.

[24] V. Akbari, S. Ghobadi, S. Mohammadi, R. Khodarahmi, The antidepressant drug; trazodone inhibits Tau amyloidogenesis: prospects for prophylaxis and treatment of AD, Arch. Biochem. Biophys. 679 (2020), 108218.

[25] W.-C. Ko, C.-M. Shih, Y.-H. Lai, J.-H. Chen, H.-L. Huang, Inhibitory effects of flavonoids on phosphodiesterase isozymes from guinea pig and their structure–activity relationships, Biochem. Pharmacol. 68 (2004) 2087–2094.

[26] E. Corradini, P. Foglia, P. Giansanti, R. Gubbiotti, R. Samperi, A. Laganà, Flavonoids: chemical properties and analytical methodologies of identification and quantitation in foods and plants, Nat. Prod. Res. 25 (2011) 469–495.

[27] R.A. Dixon, D. Ferreira, Genistein, Phytochemistry 60 (2002) 205–211.

[28] C.E. Gleason, B.L. Fischer, N.M. Dowling, K.D.R. Setchell, C.S. Atwood, C. M. Carlsson, S. Asthana, Cognitive effects of soy isoflavones in patients with Alzheimer's disease, J. Alzheimer's Dis. 47 (2015) 1009–1019.

[29] D.T. Zava, G. Duwe, Estrogenic and antiproliferative properties of genistein and other flavonoids in human breast cancer cells in vitro, Nutr. Cancer 27 (1997) 31–40.

[30] L.-X. Liu, W.-F. Chen, J.-X. Xie, M.-S. Wong, Neuroprotective effects of genistein on dopaminergic neurons in the mice model of Parkinson's disease, Neurosci. Res. 60 (2008) 156–161.

[31] M. Sonee, T. Sum, C. Wang, S.K. Mukherjee, The soy isoflavone, genistein, protects human cortical neuronal cells from oxidative stress, NeuroToxicology 25 (2004) 885–891.

[32] D.R. Gargi Chatterjee, Vineet Kumar Khemka, Mrittika Chattopadhyay, Sasanka Chakrabarti, Genistein, the Isoflavone in Soybean, Causes Amyloid Beta Peptide Accumulation in Human Neuroblastoma Cell Line: Implications in Alzheimer's Disease, Aging and Dis. 6 (2015) 456-465.

[33] B. Ren, Y. Liu, Y. Zhang, Y. Cai, X. Gong, Y. Chang, L. Xu, J. Zheng, Genistein: A dual inhibitor of both amyloid β and human islet amylin peptides, ACS Chem. Neurosci. 9 (2018) 1215–1224.

[34] K.P. Devi, B. Shanmuganathan, A. Manayi, S.F. Nabavi, S.M. Nabavi, Molecular and therapeutic targets of genistein in Alzheimer's disease, Mol. Neurobiol. 54 (2017) 7028–7041.

[35] Y.P. Shentu, W.T. Hu, J.W. Liang, Z.Y. Liuyang, H. Wei, W. Qun, X.C. Wang, J. Z. Wang, J. Westermarck, R. Liu, Genistein decreases APP/tau phosphorylation and ameliorates Aβ overproduction through inhibiting CIP2A, Curr. Alzheimer Res. 16 (2019) 732–740.

[36] J. Wei, F. Yang, C. Gong, X. Shi, G. Wang, Protective effect of daidzein against streptozotocin-induced Alzheimer's disease via improving cognitive dysfunction and oxidative stress in rat model, J. Biochem. Mol. Toxicol. 33 (2019), e22319.

[37] H.T.T. Phan, K. Samarat, Y. Takamura, A.F. Azo-Oussou, Y. Nakazono, M.d. C. Vestergaard, Polyphenols modulate Alzheimer's amyloid beta aggregation in a structure-dependent manner, Nutrients 11 (2019) 756.

[38] S. Andarzi Gargari, A. Barzegar, A. Tarinejad, The role of phenolic OH groups of flavonoid compounds with H-bond formation ability to suppress amyloid mature fibrils by destabilizing β-sheet conformation of monomeric Aβ17-42, PLoS ONE 13 (2018), e0199541.

[39] S.J. Basha, P. Mohan, D.P. Yeggoni, Z.R. Babu, P.B. Kumar, A.D. Rao, R. Subramanyam, A.G. Damu, New flavone-cyanoacetamide hybrids with a combination of cholinergic, antioxidant, modulation of β-amyloid aggregation, and neuroprotection properties as innovative multifunctional therapeutic candidates for Alzheimer's disease and unraveling their mechanism of action with acetylcholinesterase, Mol. Pharmaceutics 15 (2018) 2206–2223.

[40] A.S. DeToma, J. Krishnamoorthy, Y. Nam, H.J. Lee, J.R. Brender, A. Kochi, D. Lee, V. Onnis, C. Congiu, S. Manfredini, S. Vertuani, G. Balboni, A. Ramamoorthy, M. H. Lim, Interaction and reactivity of synthetic aminoisoflavones with metal-free and metal-associated amyloid-β, Chem. Sci. 5 (2014) 4851–4862.

[41] G. Nam, Y. Ji, H.J. Lee, J. Kang, Y. Yi, M. Kim, Y. Lin, Y.-H. Lee, M.H. Lim, Orobol: an isoflavone exhibiting regulatory multifunctionality against four pathological features of Alzheimer's disease, ACS Chem. Neurosci. 10 (2019) 3386–3390.

[42] K.J. Korshavn, M. Jang, Y.J. Kwak, A. Kochi, S. Vertuani, A. Bhunia, S. Manfredini, A. Ramamoorthy, M.H. Lim, Reactivity of metal-free and metal-associated amyloid-β with glycosylated polyphenols and their esterified derivatives, Sci. Rep. 5 (2015) 17842.

[43] X. He, H.M. Park, S.-J. Hyung, A.S. DeToma, C. Kim, B.T. Ruotolo, M.H. Lim, Exploring the reactivity of flavonoid compounds with metal-associated amyloid-β species, Dalton Trans. 41 (2012) 6558–6566.

[44] A.S. DeToma, J.-S. Choi, J.J. Braymer, M.H. Lim Myricetin, A naturally occurring regulator of metal-induced amyloid-β aggregation and neurotoxicity, ChemBioChem 12 (2011) 1198–1201.

[45] M.G. Savelieff, G. Nam, J. Kang, H.J. Lee, M. Lee, M.H. Lim, Development of multifunctional molecules as potential therapeutic candidates for Alzheimer's disease, parkinson's disease, and amyotrophic lateral sclerosis in the last decade, Chem. Rev. 119 (2019) 1221–1322.

[46] L.E. Scott, C. Orvig, Medicinal inorganic chemistry approaches to passivation and removal of aberrant metal ions in disease, Chem. Rev. 109 (2009) 4885–4910.

[47] C. Hureau, I. Sasaki, E. Gras, P., Faller two functions, one molecule: a metal-binding and a targeting moiety to combat Alzheimer's disease, ChemBioChem 11 (2010) 950–953.

[48] A. Espargaró, T. Ginex, M.d.M. Vadell, M.A. Busquets, J. Estelrich, D. Muñoz-Torrero, F.J. Luque, R. Sabate, Combined in Vitro Cell-Based/in Silico Screening of Naturally Occurring Flavonoids and Phenolic Compounds as Potential Anti-Alzheimer Drugs, J. Nat. Prod. 80 (2017) 278-289.

[49] Y. Soeda, M. Yoshikawa, O.F.X. Almeida, A. Sumioka, S. Maeda, H. Osada, Y. Kondoh, A. Saito, T. Miyasaka, T. Kimura, M. Suzuki, H. Koyama, Y. Yoshiike, H. Sugimoto, Y. Ihara, A. Takashima, Toxic tau oligomer formation blocked by capping of cysteine residues with 1,2-dihydroxybenzene groups, Nat. Commun. 6 (2015) 10216.

[50] J.M. Levenson, S. Schroeter, J.C. Carroll, V. Cullen, E. Asp, M. Proschitsky, C.H.-Y. Chung, S. Gilead, M. Nadeem, H.B. Dodiya, S. Shoaga, E.J. Mufson, H. Tsubery, R. Krishnan, J. Wright, B. Solomon, R. Fisher, K.S. Gannon, NPT088 reduces both amyloid-β and tau pathologies in transgenic mice, Alzheimer's & Dementia 2 (2016) 141–155.

[51] X.L. Shi, N. Yan, Y.J. Cui, Z.P. Liu, A Unique GSK-3beta inhibitor B10 Has a Direct Effect on Abeta, Targets Tau and Metal Dyshomeostasis, and Promotes Neuronal Neurite Outgrowth, Cells 9 (2020) 649.

[52] M.A. Selepe, F.R. Van Heerden, Application of the Suzuki-Miyaura Reaction in the Synthesis of Flavonoids, Molecules 18 (2013) 4739–4765.

[53] A. Franko, D.C. Rodriguez Camargo, A. Böddrich, D. Garg, A. Rodriguez Camargo, B. Rathkolb, D. Janik, M. Aichler, A. Feuchtinger, F. Neff, H. Fuchs, E.E. Wanker, B. Reif, H.-U. Häring, A. Peter, M., Hrabě de Angelis, Epigallocatechin gallate (EGCG) reduces the intensity of pancreatic amyloid fibrils in human islet amyloid polypeptide (hIAPP) transgenic mice, Sci. Rep. 8 (2018) 1116.

[54] S.-J. Hyung, A.S. DeToma, J.R. Brender, S. Lee, S. Vivekanandan, A. Kochi, J.-S. Choi, A. Ramamoorthy, B.T. Ruotolo, M.H. Lim, Insights into antiamyloidogenic properties of the green tea extract (−)-epigallocatechin-3-gallate toward metal-associated amyloid-β species, Proc. Natl. Acad. Sci. U.S.A. 110 (2013) 3743–3748.

[55] D.E. Ehrnhoefer, J. Bieschke, A. Boeddrich, M. Herbst, L. Masino, R. Lurz, S. Engemann, A. Pastore, E.E. Wanker, EGCG redirects amyloidogenic polypeptides into unstructured, off-pathway oligomers, Nat. Struct. Mol. Biol. 15 (2008) 558–566.

[56] B. Zhang, X.R. Cheng, I.S. da Silva, V.W.S. Hung, A.J. Veloso, L. Angnes, K. Kerman, Electroanalysis of the interaction between (−)-epigallocatechin-3-gallate (EGCG) and amyloid-β in the presence of copper, Metallomics 5 (2013) 259–264.

[57] J. Habchi, S. Chia, R. Limbocker, B. Mannini, M. Ahn, M. Perni, O. Hansson, P. Arosio, J.R. Kumita, P.K. Challa, S.I.A. Cohen, S. Linse, C.M. Dobson, T.P. J. Knowles, M. Vendruscolo, Systematic development of small molecules to inhibit specific microscopic steps of Aβ42 aggregation in Alzheimer's disease, Proc. Natl. Acad. Sci. U.S.A. 114 (2017) E200–E208.

[58] C. Dammers, L. Gremer, P. Neudecker, H.-U. Demuth, M. Schwarten, D. Willbold, Purification and characterization of recombinant N-terminally pyroglutamate-modified amyloid-β variants and structural analysis by solution NMR spectroscopy, PLoS ONE 10 (2015), e0139710.

[59] G. Bellomo, S. Bologna, L. Gonnelli, E. Ravera, M. Fragai, M. Lelli, C. Luchinat, Aggregation kinetics of the Aβ1–40 peptide monitored by NMR, Chem. Commun. 54 (2018) 7601–7604.

[60] A. Sillen, A. Leroy, J.-M. Wieruszeski, A. Loyens, J.-C. Beauvillain, L. Buée, I. Landrieu, G. Lippens, Regions of tau implicated in the paired helical fragment core as defined by NMR, ChemBioChem 6 (2005) 1849–1856.

[61] O. Schweers, E.M. Mandelkow, J. Biernat, E. Mandelkow, Oxidation of cysteine-322 in the repeat domain of microtubule-associated protein tau controls the in vitro assembly of paired helical filaments, Proc. Natl. Acad. Sci. U.S.A. 92 (1995) 8463–8467.

[62] T.K. Karikari, D.A. Nagel, A. Grainger, C. Clarke-Bland, E.J. Hill, K.G. Moffat, Preparation of stable tau oligomers for cellular and biochemical studies, Anal. Biochem. 566 (2019) 67–74.

[63] N. Kim, J. Do, I.G. Ju, S.H. Jeon, J.K. Lee, M.S. Oh, Picrorhiza kurroa prevents memory deficits by inhibiting NLRP3 inflammasome activation and BACE1 expression in 5xFAD mice, Neurotherapeutics 17 (2020) 189–199.

[64] J. Do, N. Kim, S.H. Jeon, M.S. Gee, Y.J. Ju, J.H. Kim, M.S. Oh, J.K. Lee, Trans-cinnamaldehyde alleviates amyloid-beta pathogenesis via the SIRT1-PGC1alpha-PPARgamma pathway in 5XFAD transgenic mice, Int. J. Mol. Sci. 21 (2020) 4492.

[65] A.S. Kumar, R.A. Kumar, V. Satyanarayana, E.P. Reddy, B.J.M. Reddy, D.N. Kumar, A. Khurana, G. Chandraiah, J.S. Yadav, Catalyst-Free Synthesis of Novel 6-Phenyl-6H-chromeno [4, 3-b] quinoline Derivatives at RT: Their Further Structure Evaluation Leads to Potential Anti-cancer Agents, Nat. Prod. Commun. 12 (2017) 1934578X1701200732.

[66] J. Le Bras, J. Muzart, Palladium-catalyzed domino dehydrogenation/heck-type reactions of carbonyl compounds, Adv. Synth. & Catalysis 360 (2018) 2411–2428.

[67] Y.M. Kim, H.-S. Yoo, S.H. Son, G.Y. Kim, H.J. Jang, D.H. Kim, S.D. Kim, B.Y. Park, N.-J. Kim, A Novel Approach to N-Tf 2-Aryl-2,3-Dihydroquinolin- 4(1H)-ones via a Ligand-Free Pd(II)-Catalyzed Oxidative Aza-Michael Cyclization, Eur. J. Org. Chem. 2021 (2021) 618–622.

[68] G. Leshem, M. Richman, E. Lisniansky, M. Antman-Passig, M. Habashi, A. Gräslund, S. Wärmländer, S. Rahimipour, Photoactive chlorin e6 is a multifunctional modulator of amyloid-β aggregation and toxicity via specific interactions with its histidine residues, Chem. Sci. 10 (2019) 208–217.